Mon. Not. R. Astron. Soc. **329,** 367–376 (2002)

Investigating the central engine of ultraluminous infrared galaxies: near-infrared imaging

R. I. Davies,[1★] A. Burston[2] and M. J. Ward[2]

[1]*Max-Planck-Institut für extraterrestrische Physik, Postfach 1312, 85741 Garching, Germany*
[2]*Astronomy Department, University of Leicester, University Road, Leicester LE1 7RH*

Accepted 2001 September 10. Received 2001 August 27; in original form 2000 December 22

ABSTRACT

We present 0.5-arcsec-resolution near-infrared images of six ultraluminous infrared galaxies with known redshifts. Six of the eight bright nuclei are resolved on kiloparsec scales, suggesting that there is significant circumnuclear star formation or close progenitor nuclei. At this spatial resolution, the nuclei have very red colours that cannot in general be reproduced by reddening stellar light, but require an additional component of hot dust emission. In five of the six primary nuclei more than 20 per cent of the *K*-band continuum originates in hot dust, but the temperature cannot be determined by *JHK* broad-band colours alone. Comparison with the spectral shapes, however, does allow the temperature to be constrained, and we find in every case that it is at the upper end of the permissible range, $\gtrsim 1000$ K. This does not necessarily imply that there is an active galactic nucleus present, since there is evidence that stellar processes can also generate dust this hot via stochastic heating of small grains. The quantities of hot dust we have found here can make up to 0.5-mag difference to the *K*-band magnitude even at $z \sim 1$, with implications for observations and population synthesis models of higher-redshift objects. Observations in the *L* or *M* bands, where hot dust is most important at $z \sim 1$, could help to discriminate between models of dusty starbursts and ellipticals.

Key words: galaxies: active – galaxies: interactions – galaxies: nuclei – galaxies: Seyfert – galaxies: starburst – infrared: galaxies.

1 INTRODUCTION

Since ultraluminous infrared galaxies (ULIRGs) were first recognized, one of the major questions has been concerned with the power source. How much an active galactic nucleus (AGN) contributes to the total luminosity of a ULIRG is an important factor to consider if the physical processes occurring in galaxy interactions and evolution are to be properly understood. In their review, Sanders & Mirabel (1996) show that the fraction of Seyferts (classified by optical spectra from the literature) increases at higher luminosities, although only to 34 per cent for $\log(L_{\rm IR}/{\rm L}_\odot) = 12.0-12.5$, the most extreme regime they considered. This predominance of star formation is supported by Genzel et al. (1998) who, based on the mid-infrared emission, concluded that 70–80 per cent of ULIRGs are powered mostly by massive young stars, although it is likely that more than half of them also host an AGN. Interestingly, the results of an optical spectroscopic survey by Veilleux et al. (1995) suggested a high fraction of AGN at high luminosities: 42 per cent at $\log(L_{\rm IR}/{\rm L}_\odot) = 11-12$, increasing to 62 per cent at $\log(L_{\rm IR}/{\rm L}_\odot) > 12$. Since optical emission lines probe to a much lower optical depth than infrared and radio diagnostics, one might instead have expected fewer AGN to be found in this study.

Given these differing conclusions for larger statistical samples, more detailed studies of individual objects may be more expedient in analysing the AGN contribution to the ULIRG power source. We have obtained both spectroscopic and imaging data of a small number of ULIRGs, focusing on the near-infrared regime as it represents a good compromise between the shorter wavelengths (optical, short X-ray) where attenuation owing to dust is significant, and longer wavelengths (mid- to far-infrared) where spatial resolution is limited. The spectroscopic data are discussed in Burston, Ward & Davies (2001, referred to as Paper I hereafter) with particular reference to the line diagnostics. Paper I also provides details of how the sample was chosen and gives relevant parameters for the objects. In this paper, we concentrate more on the question of whether the *JHK* colours and continuum slope are useful in searching for hidden AGN.

Many imaging studies have tended to concentrate on morphology rather than fluxes. For example, Murphy et al. (1996) obtained both *R*- and *K*-band images of a sample of 45 ULIRGs out to $z = 0.18$, which they combined with spectroscopic redshifts to study morphologies and the incidence of interaction. Unfortunately, their data are not flux calibrated and do not yield

★E-mail: davies@mpe.mpg.de

© 2002 RAS

optical–infrared colour for these objects. However, some studies have investigated ULIRG colours. Carico et al. (1990) measured *JHK* magnitudes in 2.5-arcsec apertures for nine objects, finding colours ranging from those of normal galaxies to much redder colours suggestive of significant hot dust contributions. Sanders et al. (1988) also found evidence for very red colours in a sample of ULIRGs, even in relatively large 5-arcsec apertures. They attributed most of these to AGN on the basis of broad Hα lines; but whether all their objects are powered predominantly by an AGN or whether the Hα line is broadened by another process (e.g. a superwind) is unclear. Scoville et al. (2000) presented high-resolution data for nine luminous and 15 ultraluminous galaxies, and found that in 1.1-arcsec apertures they mostly have colours $J-H > 1$ and $H-K > 1$, requiring either reddened starlight and/or hot dust. However, none of these studies took the necessary step of combining spectroscopic and imaging data.

This paper is organized as follows. After outlining the observations and data reduction in Section 2 we discuss the size and number of bright nuclei (Section 3) and the results of aperture and annular photometry (Section 4). Then in Section 5 we fit the data with models consisting of a reddened stellar population and a hot dust component. In Section 6 we discuss whether this allows them to be categorized as AGN. The red colours of the nuclei are discussed in the context of extremely red objects (EROs) in Section 7. Conclusions are given in Section 8.

2 OBSERVATIONS AND DATA REDUCTION

Images of six ULIRGs were obtained as part of the UK Infrared Telescope (UKIRT) service observing programme on the nights of 1999 September 4, 6. Although the seventh object in the sample of Paper I (IRAS 16487 + 5447) was observed on a different night, the image quality was extremely poor and so the data were not used. The UKIRT Fast-Track Imager (UFTI), a cooled 1–2.5 μm camera with a 1024^2 HgCdTe array and a pixel scale of 0.091 arcsec, was used to obtain *J*-, *H*-, *K*-broad-band images. Standard four- or five-point dither patterns were employed to allow self-flats to be made.

The data were reduced using standard procedures in IRAF. First, the dark was subtracted from each frame. Then sky images were made by median filtering the frames and iteratively rejecting all pixels more than a few sigma above the median, and these were also subtracted. Flat-fields were made from the sky frames and divided into the object frames. For each object, the resulting frames were aligned on stars in the 90-arcsec field and then median filtered. The final images had a field of view of typically 50 arcsec. Standard stars from the UKIRT list were reduced in a similar way but using the same flat-field.

The resolution was estimated using stars in the object fields as 0.38–0.60 arcsec in *K*, increasing to 0.52–0.66 arcsec in *J*. PSFs were modelled using a Moffat profile because it fits the wings of the point spread function (PSF) far better than a Gaussian. It has the form $I(r) = I_0[1 + (r/\alpha)^2]^{-\beta}$ with FWHM $2\alpha\sqrt{2^{1/\beta} - 1}$ and can be considered a more general case, of which the Gaussian is a subset. The advantage of the Moffat profile comes from its much greater versatility than the Gaussian, particularly when α and β have smaller values. In this case, decreasing β increases the strength of the wings of the PSF, while α affects the core of the profile.

3 NUCLEAR SIZES AND MULTIPLICITY

In every case the *K*-band images have the best resolution, so these have been used to estimate nuclear source sizes (with the advantage that in *K* the nuclear sources are brighter and hence show a greater contrast against the underlying galaxy light). These images are shown in Figs 1–6. For the purposes of presentation these have

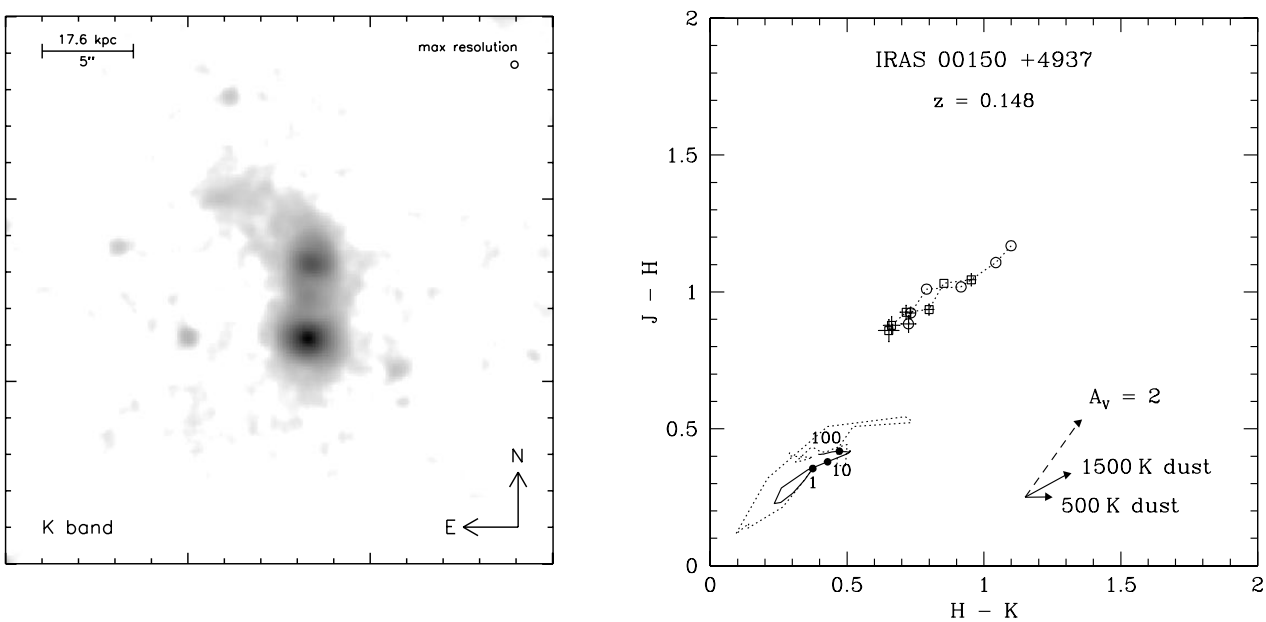

Figure 1. Left: *K*-band image of IRAS 00150 + 4937 (see text for details). The four faint objects around the galaxy are stars. Right: colour–colour diagram drawn on the same scale as Figs 1–7 for easy comparison. In the lower left of the diagram, drawn at the redshift of the galaxy, are stellar tracks from 1 to 900 Myr (solid, continuous with points marked at 1, 10 and 100 Myr; dotted, instantaneous; Leitherer et al. 1999). To the lower right are arrows showing the effect of extinction and hot dust on 100-Myr-old continuous star formation, also at the same redshift. The data for the brighter southern nucleus (open circles) is in consecutive annuli with radii 0.0–0.25, 0.25–0.5, etc. to 1.5 arcsec, from top right to lower left. Data for the second nucleus (open squares) are shown in a similar way, also to a radius of 1.5 arcsec.

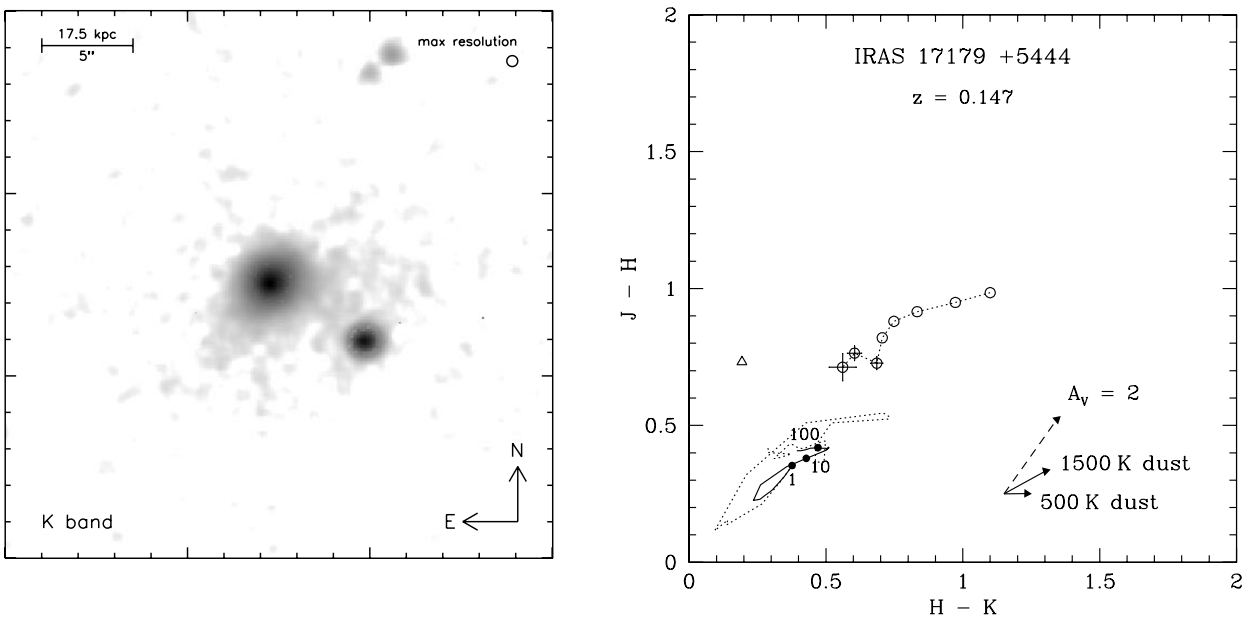

Figure 2. Left: *K*-band image of IRAS 17179 + 5444. The source to the south-west is a foreground star, as shown by its colours (open triangle in the right-hand figure). Right: colour–colour diagram as for Fig. 1. Data for the nucleus (open circles) are in consecutive annuli with radii 0.0–0.25, 0.25–0.5 arcsec, etc. to a radius of 2.5 arcsec, from top right to lower left.

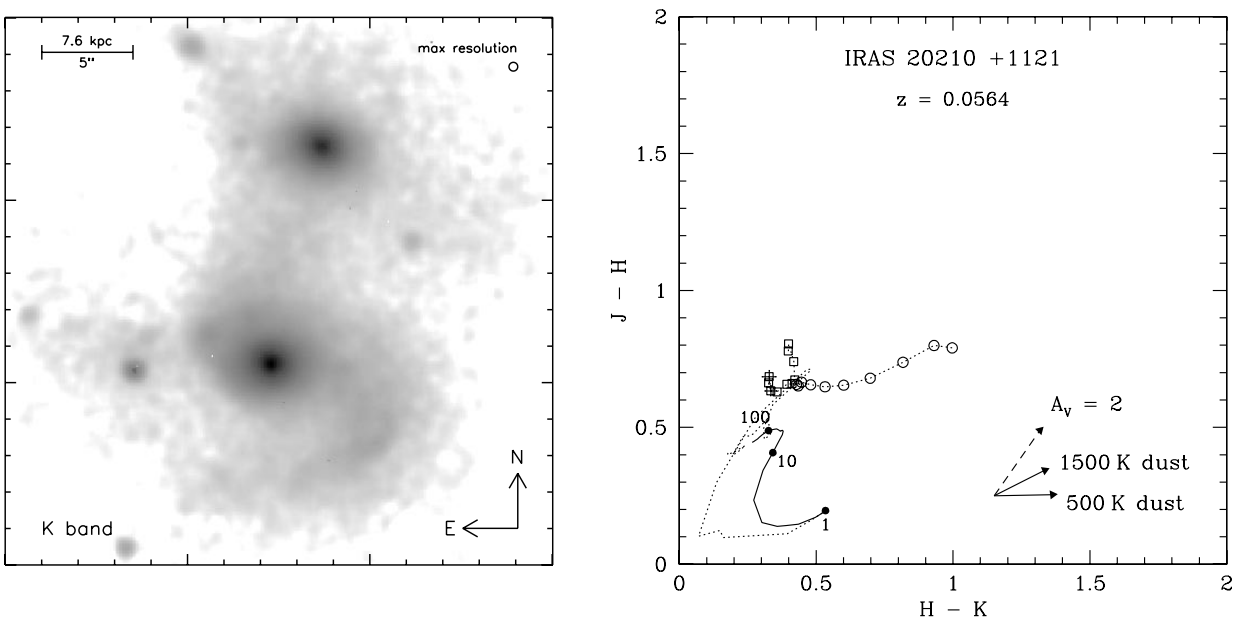

Figure 3. Left: *K*-band image of IRAS 20210 + 1121. Right: colour–colour diagram as for Fig. 1. Data for the brighter southern nucleus (open circles) are in consecutive annuli with radii 0.0–0.25, 0.25–0.5, etc. to 2.0 arcsec, from top right to lower left. Data for the second nucleus (open squares) are shown in a similar way, also to a radius of 2.0 arcsec.

been smoothed with an adaptive filter that adjusts the amount of smoothing, depending on the local signal-to-noise ratio (using the ADAPTIVE task in IRAF). Additionally, the images are displayed using a logarithmic scale. These two features allow a high dynamic range to be shown, so that both the bright nuclei and the very faint extended structure can be seen simultaneously.

The Moffat profile (see Section 2) provides a good fit to the data for the galaxy nuclei, and the sizes of the six primary nuclei and two secondary nuclei (which are no more than 2-mag fainter than the primary) are given in Table 1. What at first appears surprising is that, given the distance to these sources, most of them *are* resolved, with the only exceptions being IRAS 23498 + 2423 and the brighter nucleus of IRAS 20210 + 1121. After quadrature correcting the measured sizes for the seeing, we find typical diameters of 1–2 kpc, which argues strongly in favour of a star formation origin for at least some of the emission. However, this does not rule out the presence of an AGN since there are numerous examples of nearby galaxies that do contain an AGN and a starburst. A few objects with structure that is clearly resolved and seen to extend over 0.5–2 kpc sizes include M100 (Knapen et al. 2000),

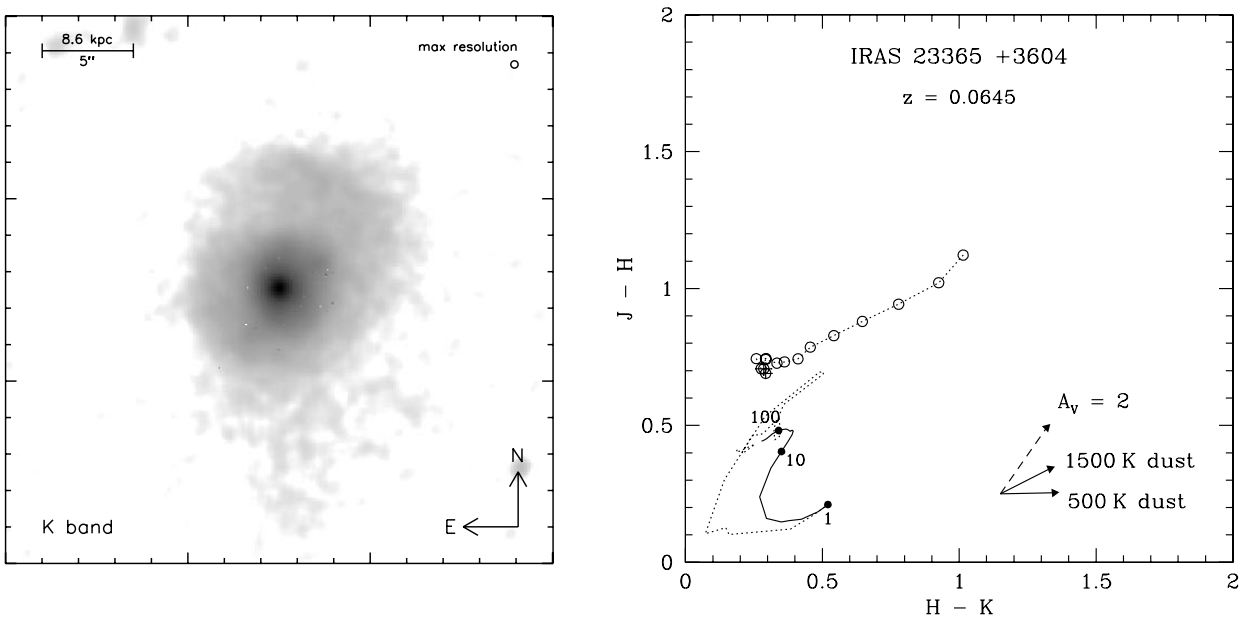

Figure 4. Left: *K*-band image of IRAS 23365 + 3604. The two faint objects to the north-east are red background galaxies. Right: colour–colour diagram as for Fig. 1. Data for the brighter southern nucleus (open circles) are in consecutive annuli with radii 0.0–0.25, 0.25–0.5, etc. to 2.5 arcsec, and then in steps of 0.5 to 5 arcsec.

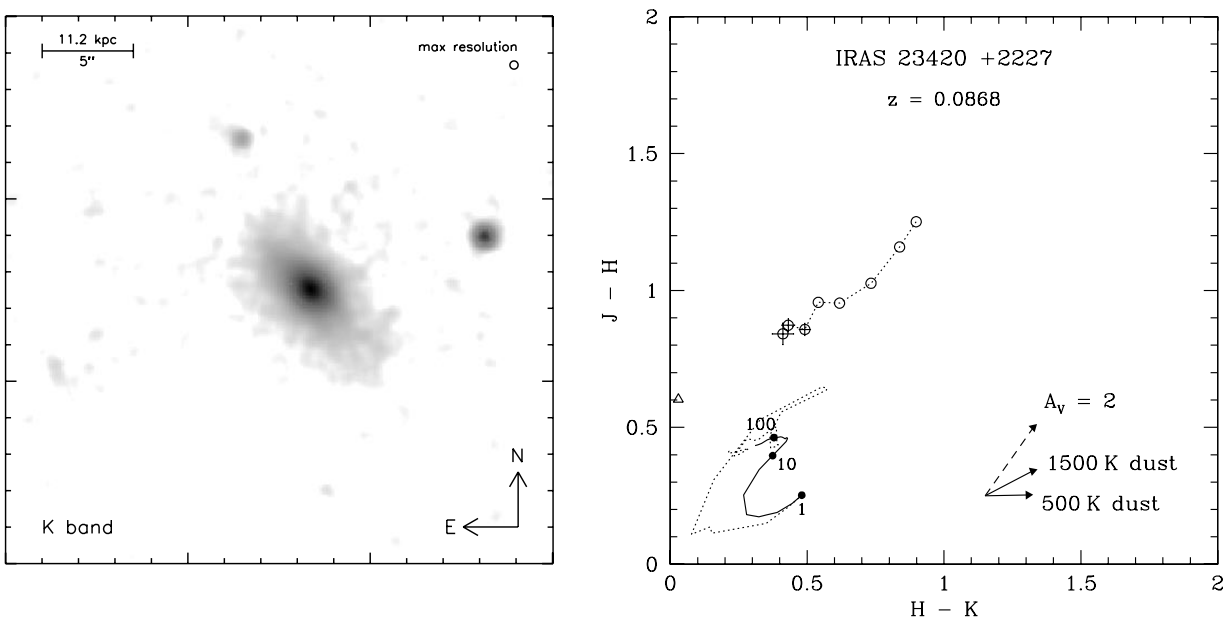

Figure 5. Left: *K*-band image of IRAS 23420 + 2227. The source to the west is a foreground star, as shown by its colours (open triangle in the right-hand figure). Right: colour–colour diagram as for Fig. 1. Data for the nucleus (open circles) are in consecutive annuli with radii 0.0–0.25, 0.25–0.5, etc. to 1.5 arcsec, and then in steps of 0.5 to 2.5 arcsec.

NGC 3351 and NGC 3504 (Planesas, Colina & Pérez-Olea 1997), NGC 1097 and NGC 6574 (Kotilainen et al. 2000), NGC 7771 (Smith et al. 1999) and NGC 7469 (Genzel et al. 1995). Based on these and other systems, typically we would expect a nuclear starburst or AGN to be confined within ∼100 pc; and a circumnuclear ring, with lower surface brightness, to have a diameter of ∼1 kpc. If observed at higher redshift, the sum of these structures would become more like a single extended region of enhanced emission. Thus being able to resolve some nuclei in the way we have done should not be unexpected. Similarly, sufficiently close progenitor nuclei in a merger remnant could appear as a single core.

Four of the galaxies we have observed are in the sample of Leech et al. (1994). These authors classified 42 luminous and ultraluminous infrared galaxies on a seven-point scale, denoting their interaction class according to *R*-band images. Of these, they concluded that 28 are interacting or merging, four have close companions but no signs of interaction, and 10 are isolated or have only distant companions. Such a large fraction of apparently non-interacting galaxies is surprising, given the commonly held view that it is interactions that drive the star formation in the most luminous galaxies. Auriére et al. (1996) also imaged three of these objects but did not draw significantly different conclusions. Two of

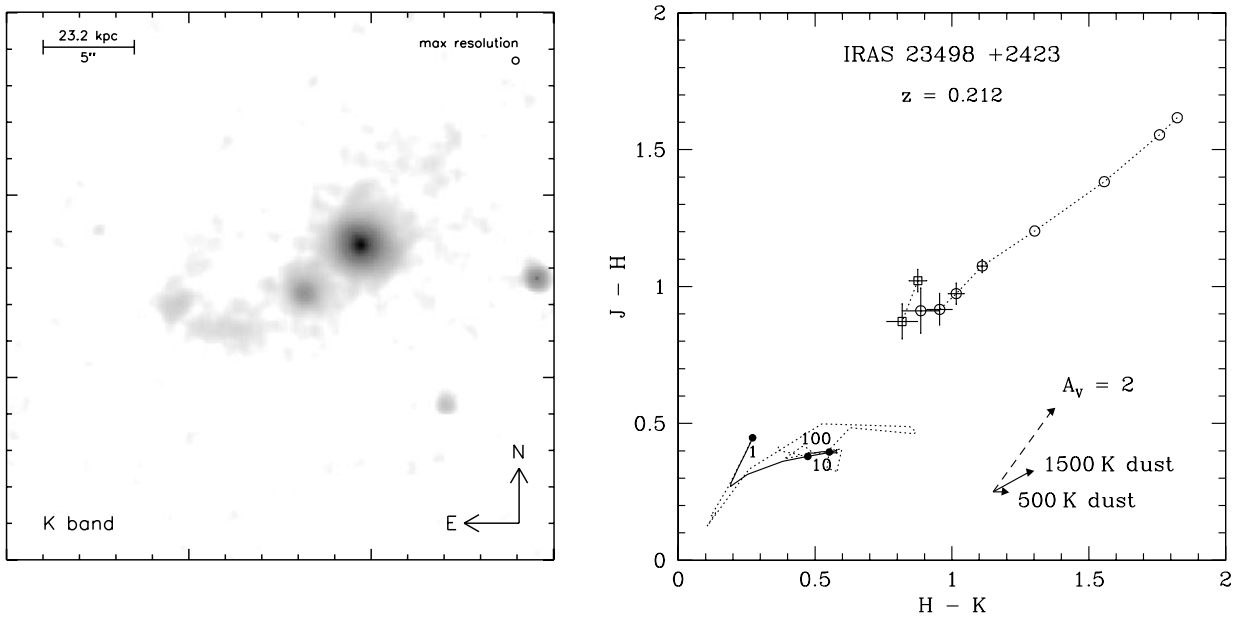

Figure 6. Left: *K*-band image of IRAS 23498 + 2423. Right: colour–colour diagram as for Fig. 1. Data for the brighter southern nucleus (open circles) are in consecutive annuli with radii 0.0–0.25, 0.25–0.5 arcsec, etc. to a radius of 2.0 arcsec, from top right to lower left. Data for the second nucleus (open squares) are shown in a similar way with annuli of 0.0–0.5 and 0.5–1.0 arcsec.

Table 1. Nuclear sizes.

IRAS name		z	*K*-band seeing (arcsec)	Nuclear *K*-band FWHM obs. (arcsec)	quad.-corr. arcsec	pc
00150+4937	S	0.148	0.39	0.60	0.46	1600
	N			0.71	0.59	2080
17179+5444		0.147	0.60	0.80	0.53	1850
20210+1121	S	0.056	0.48	0.53	$\lesssim$0.33	$\lesssim$500
	N			0.79	0.63	950
23365+3604		0.065	0.40	0.64	0.50	850
23420+2227		0.087	0.45	0.63	0.44	980
23498+2423		0.212	0.38	0.41	$\lesssim$0.29	$\lesssim$1350

'S' and 'N' denote south and north nuclei, respectively.
Upper limits on the size have been estimated where the nuclear FWHM is less than 0.1 arcsec more than the seeing.
$H_0 = 50\,\mathrm{km\,s^{-1}\,Mpc^{-1}}$ has been used throughout.

our galaxies are classed by Leech et al. as *probably merging*: we confirm that IRAS 00150 + 4937 has two prominent nuclei separated by 4.3 arcsec (15 kpc) and a clumpy extended tail reaching another 20 kpc to the north-east; IRAS 17179 + 5444 appears to be isolated, the second nucleus being in fact a foreground star. The true nucleus is itself rather broad, and we speculate whether it may in fact contain two very close progenitor cores – high-resolution images with adaptive optics or a space telescope would be needed to confirm this. One galaxy is classed as *obviously interacting*: we show that IRAS 23498 + 2423 has a very long tail to the south-east consisting of at least four distinct knots spread over more than 10 arcsec (nearly 50 kpc). And one is classed as having *no companion within 200 kpc*: we also find IRAS 23420 + 2227 to be apparently isolated and undisturbed, with foreground stars 10 arcsec west and north. If this galaxy is an inclined spiral then it may be that gas inflow driven by a barred potential (e.g. Combes et al. 1995) is responsible for the nuclear activity. Of the other two galaxies, IRAS 20210 + 1121 is clearly interacting with a strong bridge of emission spanning the 12.3 arcsec (19 kpc) between the two nuclei; and IRAS 23365 + 3604 which, while apparently isolated, shows signs of a disturbed morphology with a spiral arm to the north and diffuse emission extending at least 14 arcsec (24 kpc) south.

4 PHOTOMETRY AND COLOURS

In order to measure colours accurately with small apertures, images of each target must be at the same resolution for all three bands. Rather than deconvolve the images, which is known to lead to uncertain photometry, those with better resolution were convolved with a Gaussian kernel to match the lowest resolution image (typically *J*-band). Table 2 gives the magnitudes and colours of each object integrated in 1- and 2-arcsec apertures, the former being dominated by the bright nucleus but not necessarily the latter. The data used for the models in Section 5.1 are those in the 1-arcsec apertures, so that in each case we include as much flux as possible while still remaining dominated by the nucleus. Since the FWHM resolution is $\sim$0.6 arcsec, this aperture is effectively seeing-limited and so is optimal for studying the nuclear colours. For that reason we prefer this approach to one using apertures of fixed physical size.

In order to map better the change in colour as a function of distance from the nucleus, the colours in Figs 1–6 have been calculated for consecutive annuli, with radii increasing by 0.25 arcsec. Thus the first point is the colours in a radius of less than 0.25 arcsec; the second point is derived from only the flux measured between radii of 0.25–0.50 arcsec; and so on. Further details pertinent to individual objects are given in the figure captions. Strong colour gradients can clearly be seen in all of the objects, with the nucleus itself being much redder than the surrounding continuum emission. Typically we find colours in the extended regions to be $J-H \sim 0.7$ and $H-K \sim 0.5$ while the nuclear colours are more like $J-H \sim 1.2$ and $H-K \sim 1.0$, each being 0.5 mag redder.

Table 2. Nuclear colours and magnitudes.

IRAS name		Common resolution[b] arcsec	Integrated colours and magnitudes[a] 1-arcsec aperture $J-H$	$H-K$	K	2-arcsec aperture $J-H$	$H-K$	K
00150+4937	S	0.52	1.13	1.06	14.71	1.08	0.98	14.13
	N		1.04	0.89	16.32	0.98	0.81	15.43
17179+5444		0.66	0.96	1.02	14.86	0.93	0.90	14.13
20210+1121	S	0.64	0.79	0.96	13.70	0.75	0.87	13.09
	N		0.80	0.40	14.77	0.75	0.41	13.95
23365+3604		0.52	1.06	0.96	14.01	0.98	0.84	13.34
23420+2227		0.57	1.19	0.86	14.64	1.10	0.78	14.02
23498+2423		0.66	1.58	1.78	13.63	1.46	1.66	13.18

[a] Statistical errors are less than 0.01 mag for magnitudes brighter than 16. This includes all sources of uncertainty (photon noise, position on the detector, changes in airmass, etc.) except those of the standard stars themselves that are also less than 0.01 mag.
[b] The poorest seeing of each set of images, typically *J* band. The other two bands were convolved to this resolution.

5 STAR FORMATION, DUST AND EXTINCTION

We interpret the colours under the assumption that the near-infrared emission is dominated by two main components: stellar light and hot dust emission, both of which suffer the same extinction. Any AGN is not seen directly at these wavelengths but is expected to contribute to the hot dust component, which may also have a contribution from a young starburst. Both a starburst and a (more evolved) underlying stellar population are expected to make up the total stellar light – the near-infrared colours of which are fairly insensitive to the stellar types, and depend rather more on the extinction.

One important consideration is whether the hot dust component should be reddened, which in turn depends on the assumed geometry: whether it is the hot dust close to the AGN or star cluster that is responsible for the extinction, or whether most of the extinction is caused by cooler dust further away. In fact, it makes little difference to the results of our models which of these options is adopted – the extinction and dust fraction change by less than 10 per cent. The reason is simply that the dust makes little contribution to the total *J*- and *H*-band emission where the effects of extinction are greater.

5.1 Modelling the colours

We have calculated the colours of star formation models at the redshift of each galaxy using spectra from the STARBURST 99 models (Leitherer et al. 1999) for solar metallicity and a Salpeter initial mass function (IMF). As shown later, this choice of metallicity and IMF is not critical because the *JHK* colours are relatively insensitive to the stellar population; it provides a reasonable baseline in the absence of more detailed information concerning the galaxies. The spectra were integrated over the *JHK* bands using the transmission curves for the standard Mauna Kea near-infrared filters, with zero points derived from the spectrum of Vega (kindly provided by W. Vacca). The loci are drawn in Figs 1–6, where the solid lines represent continuous star formation, and the dotted lines represent instantaneous star formation; the effect responsible for the *K*-correction can easily be seen. The age range is from 1 to 900 Myr, but at ages greater than ~ 20 Myr the colours change very little. For the purposes of matching the observed colours, we have made the plausible assumption that the star formation has been continuous over 100 Myr (and demonstrate later that this is actually not critical). The rationale is provided by the hypothesis that the star formation history in ULIRGs has been punctuated by multiple episodes of star formation in individual star clusters (or groups of clusters) spread over a significant (up to several 100 Myr) time-scale, similar to the interaction time-scale. This is effectively a model for quasi-continuous star formation. Additionally, in each of Figs 1–6 we have drawn the vectors indicating the effect at the appropriate redshift, of hot dust at 500 and 1500 K contributing a fraction $f_{K\mathrm{d}} = 0.3$ of the rest-frame *K*-band emission (the underlying spectrum is that of a 100-Myr stellar population), and extinction (screen model) with $A_V = 2$. We favour the screen model in this instance because we are mostly concerned with the galaxy nuclei in which the source is expected to be either an AGN or a number of bright compact stellar clusters. It seems reasonable to assume that the bulk of the dust responsible for the extinction is surrounding rather than intrinsic to these structures. Indeed, attempts to use the 'mixed dust model', in which the dust is mixed with the stars, frequently give rms errors of greater than 0.15 mag between the model and the data. Scoville et al. (2000) also considered the mixed dust model and their figs 5–7 show that for low extinctions (i.e. typically the regime here – see below and Table 3), although the estimated optical depth for the mixed model is 2–3 times greater than the screen model, there is, in fact, not much difference in the effect on the colours.

Table 3. Model parameters.

IRAS name		$f_{K\mathrm{d}}$[a]	A_V[a]	rms[b]
00150+4937	S	0.21 ± 0.04	5.06 ± 0.17	0.00
	N	0.00 ± 0.00	4.47 ± 0.00	0.02
17179+5444		0.38 ± 0.05	3.56 ± 0.41	0.00
20210+1121	S	0.57 ± 0.10	1.19 ± 1.00	0.02
	N	0.00 ± 0.00	2.02 ± 0.00	0.12
23365+3604		0.36 ± 0.08	4.14 ± 0.56	0.00
23420+2227		0.00 ± 0.00	5.70 ± 0.00	0.03
23498+2423		0.77 ± 0.11	5.86 ± 2.77	0.02

[a] Mean and uncertainty estimated for hot dust temperatures in the range 500–1500 K, for 100 Myr continuous star formation with solar metallicity.
[b] Mean rms of the differences in $J-H$ and $H-K$ between the models and data.

We find that the extended emission is consistent with an old ($\gtrsim 100$ Myr) stellar population with $A_V \sim 2$, while the nuclear

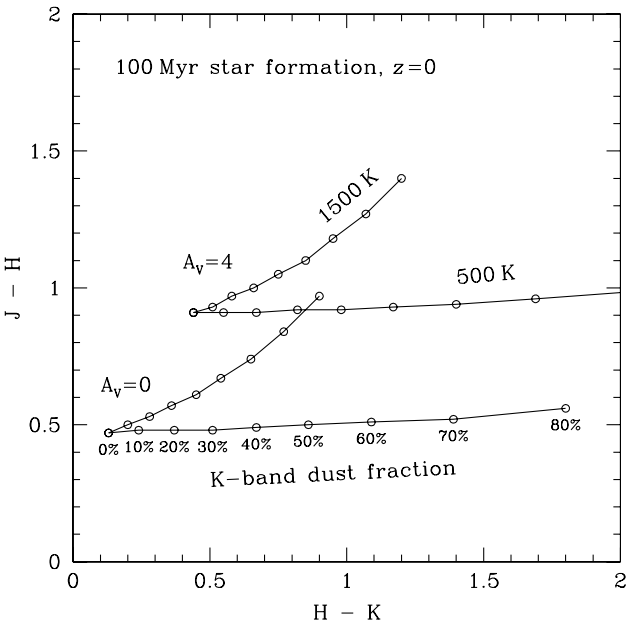

Figure 7. The effect of dust and extinction on 100-Myr-old star formation at $z = 0$ with no extinction (lower set of lines) and $A_V = 4$ reddening both stars and hot dust (upper set of lines). Two dust temperatures, 500 and 1500 K, are considered, and added so that 0–80 per cent of the *K*-band flux is from the hot dust. This figure is drawn on the same scale as Figs 1–6 for ease of comparison.

colours require both more extinction and significant emission from hot dust. The argument is essentially that, starting from the locus of colours traced by star clusters, it is not in general possible to attain the colours observed in the nucleus by extinction alone; the nuclei have too large an $H-K$ colour, and this requires a contribution to the emission from hot dust. To investigate this quantitatively we have modelled the nuclear colours with 100-Myr-old continuous star formation to which is added a contribution from dust at 500–1500 K, both reddened by an extinction screen. The temperature range provides two extremes: at 500 K the dust changes only the $H-K$ colour so the derived extinction is maximal; while 1500 K is close to the sublimation temperature of grains and represents the case of minimal extinction. This is demonstrated in Fig. 7 which shows that, for example, a galaxy at $z = 0$ with $H-K = 0.9$ and $J-H = 0.9$ can have extinction in the range $A_V = 0$–4. In the first case $f_{Kd} = 0.75$ with a dust temperature of 1500 K; in the latter case $f_{Kd} = 0.3$ at 500 K.

The results of modelling the colours in the inner 1 arcsec of eight nuclei in these *IRAS* galaxies are given in Table 3. The best fit was found using a χ^2 minimization; but because in many cases it was possible to match the data exactly, the goodness of fit is indicated by a simple rms difference between this and the data. The 1σ variation introduced by a change of 0.02 mag in the $J-H$ and $H-K$ colours is less than ± 0.02 for f_{Kd} and ± 0.12 for A_V. In order to assess the effect of our assumption for 100-Myr-old star formation we have applied a model with 1000-K dust using ages that are up to a factor of 5 more and less, 20–500 Myr. The variation this causes is less than ± 0.06 for f_{Kd} and ± 0.20 for A_V. Similarly, varying the metallicity from 0.4 to 2.0 $Z_\odot$ does not introduce much variation, typically ± 0.03 for f_{Kd} and ± 0.30 for A_V. The reason is simply that near-infrared colours are not particularly sensitive to variations in the stellar population, and any changes tend to be damped out anyway if there is a large contribution from dust to the total emission. Thus our results, which we summarize below, appear to be fairly robust.

The extinction is a little greater than that of the extended emission, typically $A_V = 3$–6. This does not contradict the much larger values measured in the mid-infrared (e.g. Genzel et al. 1998) because the longer wavelengths probe to greater optical depths, and we can only consider the extinction to the stars responsible for the observable near-infrared emission.

For five of the eight nuclei (and five of the six primary nuclei) a significant fraction, 20–80 per cent, of the *K*-band flux is caused by dust emission. This is similar to the result found by Surace, Sanders & Evans (2000) that most ULIRG nuclei have colours consistent with a young stellar population combined with hot dust that contributes 30–40 per cent of the K' flux. That dust should play such an important role in the near-infrared should not be unexpected since the enormous far-infrared luminosity that classifies these objects as ULIRGs is itself evidence for the presence of large quantities of dust.

5.2 Comparison with spectra

To strengthen this result, we can argue that the *H*- and *K*-band spectral shapes [that Burston et al. (2001) present] rule out models relying solely on extinction. First, we consider stellar populations with reddening determined from emission lines (Burston et al. 2001), typically $A_V \lesssim 4$: the *K*-band slopes of these are not red enough to match the observed continua. Secondly, the largest optical depth at which we expect to see emission at a wavelength λ is $\tau_\lambda \sim 1$, corresponding to $A_V \sim 10$ for the *K* band and a little less for the *H* band. Some of our objects have *K*-band slopes consistent with this model. However, stellar populations for such high extinctions have a characteristic shape: rising to longer wavelengths in the *H* band before falling again in the *K* band. None of the *H*-band spectra match this, instead being much flatter (except IRAS 23498 + 2423 which is steeper). Thus it is inevitable that a component of dust emission is required to fit the continuum shape between 1.5 and 2.4 μm.

Furthermore, the spectral shapes can also overcome some of the degeneracy between extinction and hot dust emission that stopped us from being able to determine the dust temperature. As demonstrated for two examples in Davies, Burston & Ward (2000), the reason is that dust at ~500 K has a characteristic rise towards the longer end of the *K* band, which is not seen in any of the spectra of our sample; on the other hand, dust at $\gtrsim$1000 K rises gradually through the whole *K* band (and is, at first glance, less obvious in the spectrum). In order to compare the model with the observed spectra, we must take account of the different apertures used in the imaging and spectroscopy, since the models were fitted to colours in a 1-arcsec aperture, while the spectra were extracted over a 3-arcsec length of slit. If we do this and fit the model to colours in 2–3 arcsec apertures, then all of the *H*- and *K*-band spectra can be matched very well. We find that in each case only the models with higher-temperature ($\gtrsim$1000 K) dust emission are consistent with the spectral shapes.

6 STARBURST OR AGN?

It is an important question whether the presence of dust at $\gtrsim$1000 K must also imply the presence of an AGN. Typically, one might expect that to heat dust close to its sublimation temperature requires a very intense ultraviolet (UV) radiation field that only occurs within a few parsecs of an AGN, that is the inner edge of a

putative torus. Indeed, *Infrared Space Observatory* (*ISO*) spectroscopy of classic 'template' starburst and AGN galaxies (Sturm et al. 2000; Lutz 2000) suggests that it is only AGN that have spectral shapes indicative of dust emission at these temperatures. However, it should be noted that at 2.4–12μm the *ISO*-SWS aperture is $14 \times 20\,\mathrm{arcsec}^2$, which is large even for nearby objects and includes a significant fraction of the more extended emission associated with a galaxy bulge or disc. From Table 2 it is apparent that for all the objects (except IRAS 23498 + 2423) the *K*-band flux in a 2-arcsec aperture is at least twice that in a 1-arcsec aperture. Thus even for ULIRGs, in most cases it is not the nucleus that dominates the integrated *K*-band flux. For the *ISO* template starbursts, it is to be expected then that late-type stars might easily dominate the near-infrared emission and hide any relatively weaker hot dust emission associated only with younger star clusters.

There is also some evidence of small-grain emission, from the detection of PAH features in some ULIRGs (Rigopoulou et al. 1999). In particular, PAH emission at 6–10μm (e.g. as in IRAS 17179 + 5444) is caused by molecules consisting of only a few hundred atoms (Draine & Aigen 2001). These same models show that the 3-μm feature seen in some reflection nebulae characterized by colour temperatures of ∼1000 K (Sellgren, Werner & Dinerstein 1983) may be caused by PAH molecules with fewer than 100 atoms.

Sellgren (1984) explained the high colour temperatures in these nebulae in terms of stochastic heating of small grains on the order of 5–10 Å radius. The relevant results are that for a typical grain size distribution of $a^{-3.5}$ extended down to these sizes, the fraction of the dust mass in 10-Å-sized grains is 0.002, and the fraction of stellar luminosity absorbed and re-radiated by such grains is 0.004 of that absorbed and re-radiated by all grains. A simple calculation comparing the monochromatic luminosities for the dust emission at 2.2 μm with that at 60 μm (roughly corresponding to the peaks in $\nu F\nu$ for 1500 and 50 K) yields ratios of approximately 0.01, which is consistent with this model. A more robust test of the model might be to image the ULIRGs at very high resolution to determine whether the hot dust traces the distribution of young stellar clusters or is confined to one particular compact region. Measurements similar to these have been carried out by Scoville et al. (2000) who determined the colours of circumnuclear and disc clusters in infrared luminous galaxies using NICMOS on the *Hubble Space Telescope* (*HST*). A number of these clusters have colours that cannot obviously be reproduced by reddening stellar light alone, suggesting that here also there is some hot dust, although of an undetermined temperature. Spectroscopy in the *H* and *K* bands of these could show whether the temperature approaches 1500 K, which would provide strong evidence in favour of such dust existing in star clusters as well as AGN.

One argument against applying Sellgren's model to ULIRGs is that the environment in ULIRGs is rather different to that in reflection nebulae: the latter contain massive but non-ionizing stars, whereas in ULIRGs there must be ionizing stars to produce the observed hydrogen recombination emission. In this case the highest-energy UV photons from ionizing stars could destroy such small grains, or the thermal emission from the nebulae themselves could mask the small-grain emission. In the quasi-continuous star formation scheme proposed in Section 5.1 only the most recent clusters – those in which star formation has occurred within the last 10 Myr – would host ionizing stars. A significant fraction, or even the majority, of the far-infrared luminosity would still originate in these youngest ionizing clusters through thermal heating of dust grains; but the bulk of the starburst population would reside within slightly older clusters without H II regions, and these could have an observable small-grain population. There is certainly sufficient ∼1000-Å luminosity within such older clusters to produce the observed fractions of 2-μm emission via small-grain heating. Thus it is possible that in a ULIRG the necessary requisites are met so that stochastic excitation of small grains becomes an observable phenomenon.

Whatever its origin, the amounts of hot dust we have found in these ULIRGs can have an important effect on infrared diagnostics, in particular the depth of the CO absorption bands or equivalent width of Brγ ($W_{\mathrm{Br}\gamma}$). For star formation models, if $f_{K\mathrm{d}} = 0.5$ then $W_{\mathrm{Br}\gamma}$ will be underestimated by a factor of 2, with severe consequences on an age estimation of the star formation. Alternatively, if the age is constrained by other parameters, it can lead to incorrect conclusions concerning the initial mass function – such as a truncated upper mass limit or shallow slope. The most obvious way to avoid this problem is to use lines such as Paα or Paβ, where such dilution is not so serious, although this must be balanced against the higher opacities at shorter wavelengths. However, for dust at 1500 K dilution can still be severe in the *H* and even *J* bands. For dust emission superimposed on an unreddened 100-Myr-old stellar spectrum, a 50 per cent contribution from dust to the *K* band also implies 18 and 5 per cent contributions to the *H* and *J* bands, respectively.

7 EXTREMELY RED OBJECTS

Recently, there has been a great deal of interest in a population of extremely red objects (EROs), which are rather arbitrarily identified by colours $R-K \gtrsim 5-6$ or $I-K \gtrsim 4-5$. There are a number of cases that demonstrate the extragalactic nature of at least some of them (Hu & Ridgway 1994; Graham & Dey 1996; Yan et al. 2000), which have near-infrared colours $J-H \sim 1.4-1.6$ and $H-K \sim 1.0-1.2$.

There are a few cases in which the optical–infrared colours of ULIRGs have been measured, and some of these satisfy the criteria for classification as EROs; that is, it appears that some ULIRGs could form a class of low-redshift EROs. Sanders et al. (1988) presented *JHK* data and Gunn-*r* and Gunn-*i* photometry on 10 ULIRGs. Although these filters differ slightly from Johnson *R* and *I* filters, the result still stands: two of their objects had $i-K > 5$ and $r-K > 5$, while the mean colours were $i-K = 4.6 \pm 0.9$ and $r-K = 4.6 \pm 0.8$. The infrared colours were also similar to those found in EROs, and were $J-H = 1.0 \pm 0.2$, $H-K = 0.9 \pm 0.3$. All but one of our six objects have such colours, with either $J-H \gtrsim 1$ or $H-K \gtrsim 1$ and one (IRAS 23498 + 2423) is much redder still. This leads us to ask whether the extinction and hot dust, which cause ULIRGs to appear so red, can also apply at higher redshifts; that is, at what redshifts might ULIRGs contribute to the ERO phenomenon? Because extinction preferentially reduces the flux at shorter wavelengths it will have a great impact on the $R-K$ colour of a galaxy, more so at high redshift where the UV gradually shifts into the observer's *R* band. Although dust is most important in the *K* and longer bands, as we have seen that hot dust from an AGN can, in some cases, contribute significantly at shorter wavelengths and so its effects may persist to higher redshift. To examine these effects more carefully we have calculated the $R-K$ colours of stellar populations with various reddenings and 1500-K dust contributions as a function of redshift. The results are shown in Fig. 8 for continuous star formation on a time-scale of 100 Myr. With no extinction there is little colour change with redshift because the spectral energy distribution peaks shortward of the

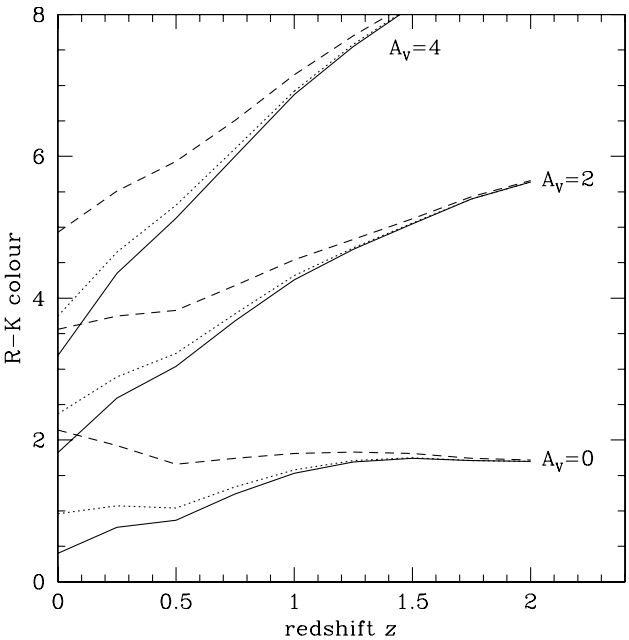

Figure 8. The $R-K$ colours expected for a 100-Myr-old burst of star formation for various extinctions as a function of redshift. The R-band magnitude was calculated using the filter transmission profile for the SUSI camera on the NTT. The solid lines have no hot dust; the dotted lines represents a contribution of 40 per cent to the rest-frame K-band flux from 1500-K dust (as expected for an AGN); the dashed lines are for a 80 per cent contribution. While it is clear that the extinction has the greatest effect on $R-K$ colour, hot dust can still redden it by up to $\sim$0.5 mag at $z = 1$.

R-band. As the extinction is increased, the peak quickly shifts to between the bands, with the result that changing the redshift has a much greater impact. The results for continuous star formation of any age are very similar because the shorter wavelengths are still dominated by hot young stars. For an old passively evolved population the colour strongly reddens with redshift because the peak in the spectral energy distribution already lies between the R and K bands. The effect of dust is, as expected, strongest at low redshift, but surprisingly can still make up to $\Delta(R-K) \sim 0.5$ mag difference at $z \sim 1$ for objects with a sufficient rest-frame K-band dust contribution.

It appears that the only way for a galaxy at $z < 0.5$ to resemble an ERO is to have relatively high extinction and a large hot dust contribution, and IRAS 23498 + 2423 (a known broad-line region AGN) is the only one of our samples that comes close to fulfilling these criteria. At higher redshifts, it is extinction or an ageing stellar population that are the defining properties. In fact, any stellar population older than 100 Myr suffering an extinction of $A_V = 4$ or more, or any population older than 1 Gyr with an extinction of $A_V > 2$, would be classified as an ERO if redshifted to $z > 1$. However, owing to the difficulty in distinguishing stellar spectra based on broad-band photometry from V to K (in the observer's frame), it is not yet clear what proportion of different stellar populations contribute to EROs. It may well be that adaptive optics systems on 8-m class telescopes, which will be more sensitive to point sources than extended objects, will find a population of very red point-like sources, perhaps representing high-redshift reddened AGN or dusty starbursts (Davies et al. 2001). Such a population could easily change the relative fractions of ellipticals and dusty starbursts that make up EROs. Additionally, to determine what fraction of them might be starbursts or AGN similar to ULIRGs we suggest searching for the signature of hot dust by observing them in their rest-frame K band, that is in the observer's frame L and M bands.

8 CONCLUSION

We present *JHK* images at $\sim$0.5-arcsec resolution of six ULIRGs with known redshifts.

Most of the nuclei in the galaxies are resolved, arguing for an extended starburst, most likely circumnuclear ring or close progenitor nuclei. We emphasize that this alone does not rule out an AGN component. We also note that foreground stars can easily be, and indeed have been, confused with a second nucleus and can only be safely identified by their colours or spectroscopic data.

The colours of the extended emission (more than a few kpc from the nucleus) are $J-H \sim 0.7$ and $H-K \sim 0.5$ similar to colours in discs of normal galaxies and consistent with a stellar population that is slightly reddened. The nuclei are redder with $J-H \sim 1.2$ and $H-K \sim 1.0$. We have modelled the nuclear colours as a combination of a reddened stellar continuum and a hot dust contribution (from a young starburst or AGN) with a temperature in the range 500–1500 K. We find that extinctions (at least to the stars responsible for the observed near-infrared emission) are moderate – $A_V = 3-6$ for a screen model – and that significant contributions from hot dust are required. In five of the eight nuclei (and five of six primary nuclei), 20–80 per cent of the K-band continuum originates in heated dust.

With *JHK* data alone the dust temperature cannot be constrained within the range used in the models. However, comparison of the model with observed spectra in the H and K bands indicates not only that dust is required, but also that the dust present is at the hotter end of the possible range with $T \gtrsim 1000$ K. Both the inner edge of the putative torus around an AGN and stochastic heating of small grains by OB stars can explain dust emission at $\gtrsim 1000$ K. Combined imaging and spectroscopic observations of off-nuclear clusters in nearby galaxies could provide evidence for whether stochastic heating of grains is indeed an important process on the scale of star clusters, or whether detection of hot dust implies the presence of an AGN.

Lastly, we have considered ULIRGS from the perspective of EROs. Many EROs are suspected to be either high-redshift ellipticals or high-redshift dusty starbursts. The hot dust that makes ULIRGs so red still affects the observer's frame K band at redshifts as high as $z \sim 1$. Adaptive optics systems on large telescopes will be sensitive to high-redshift dusty starbursts and AGN, and may find a larger population of these than is currently known. We also propose that observing EROs in the L and M bands could determine effectively whether there is much hot dust emission contributing to their colours and help to break the degeneracy in V to K broad-band photometry.

ACKNOWLEDGMENTS

The United Kingdom Infrared Telescope is operated by the Joint Astronomy Centre on behalf of the UK Particle Physics and Astronomy Research Council. The data reported here were obtained as part of the UKIRT Service Programme. RID thanks Matt Lehnert for entertaining and fruitful discussions.

REFERENCES

Auriére M., Hecquet J., Coupinot G., Arthaud R., Mirabel F., 1996, A&A, 312, 387

Burston A. J., Ward M. J., Davies R. I., 2001, MNRAS, 326, 403 (Paper I)
Carico D., Graham J., Matthews K., Wilson T., Soifer B., Neugebauer G., Sanders D., 1990, ApJ, 349, 39
Cohen J., Blandford R., Hogg D., Pahre M., Shopbell P., 1999, ApJ, 512, 30
Combes F., Boissé P., Mazure A., Blanchard A., 1995, Galaxies and Cosmology. Springer, Berlin
Davies R., Burston A., Ward M., 2000, in Tacconi L., Lutz D., eds, Starbursts Near and Far. Springer, Berlin
Davies R., Lehernt M., Baker A., Rabien S., 2001, in Schilizzi R., Vogel S., Paresce F., Elvis M., eds, Proc. IAU Symp. 205, Galaxies & their Constituents at the Highest Angular Resolutions. Astron. Soc. Pac., San Francisco
Draine B., Aigen L., 2001, ApJ, 551, 807
Eckart A., van der Werf P., Hofmann R., Harris A., 1994, ApJ, 424, 627
Genzel R., Weitzel L., Tacconi-Garman L., Blietz M., Cameron M., Krabbe A., Lutz D., Sternberg A., 1995, ApJ, 444, 129
Genzel R. et al., 1998, ApJ, 498, 579
Graham J., Dey A., 1996, ApJ, 471, 720
Hu E., Ridgway S., 1994, AJ, 107, 1303
Knapen J., Shlosman I., Heller C., Rand R., Beckman J., Rozas M., 2000, ApJ, 528, 219
Kotilainen J., Reunanen J., Laine S., Ryder S., 2000, A&A, 353, 834
Leech K., Rowan-Robinson M., Lawrence A., Hughes D., 1994, MNRAS, 267, 253
Leitherer C. et al., 1999, ApJS, 123, 3
Lutz D., 2000, New Astron. Rev., 44, 241
Murphy T., Armus L., Matthews K., Soifer B., Mazarrella J., Shupe D., Strauss M., Neugebauer G., 1996, AJ, 111, 1025
Planesas P., Colina L., Pérez-Olea D., 1997, A&A, 325, 81
Rigopoulou D., Spoon H., Genzel R., Lutz D., Moorwood A., Tran D., 1999, AJ, 118, 2625
Sanders D., Mirabel I., 1996, ARA&A, 34, 749
Sanders D., Soifer B., Elias J., Madore B., Matthews K., Neugebauer G., Scoville N., 1988, ApJ, 325, 74
Scoville N. et al., 2000, AJ, 119, 991
Sellgren K., 1984, ApJ, 277, 623
Sellgren K., Werner M., Dinerstein H., 1983, ApJ, 271, L13
Smith D., Herter T., Haynes M., Neff S., 1999, ApJ, 510, 669
Sturm E., Lutz D., Tan D., Feuchtgruber H., Genzel R., Kunze D., Moorwood A., Thornley M., 2000, A&A, 358, 481
Surace J., Sanders D., Evans A., 2000, ApJ, 529, 170
Tokunaga A., , Cox A. 1996, Astrophysical Quantities, 4th edn. AIP Press, New York
Veilleux S., Kim D.-C., Sanders D., Mazzarella J., Soifer B., 1995, ApJS, 98, 171
Yan L., McCarthy P., Weymann R., Malkan M., Teplitz H., Storrie-Lombardi L., Smith M., Dressler A., 2000, AJ, 120, 575

This paper has been typeset from a TEX/LATEX file prepared by the author.